A novel physics-informed framework for reconstruction of structural defects

Qi Li[1], Fushun Liu[2], Bin Wang[1], Dianzi Liu[3,*], Zhenghua Qian[1,*]

[1]State Key Laboratory of Mechanics and Control of Mechanical Structures, College of Aerospace Engineering, Nanjing University of Aeronautics and Astronautics, Nanjing, 210016, China

[2]College of Engineering, Ocean University of China, Qingdao 266100, China

[3]School of Engineering, University of East Anglia, UK

[*] Corresponding authors , E-mail: dianzi.liu@uea.ac.uk; qianzh@nuaa.edu.cn.

Abstract: Ultrasonic guided wave technology has played a significant role in the field of non-destructive testing as it employs acoustic waves that have advantages of high propagation efficiency and low energy consumption during the inspect process. However, theoretical solutions to guided wave scattering problems using assumptions such as Born approximation, have led to the poor quality of the reconstructed results. Moreover, scattering signals collected from industry sectors are often noised and nonstationary. To address these issues, a novel physics-informed framework (PIF) for quantitative reconstruction of defects using the integration of data-driven method with the guided wave scattering analysis has been proposed in this paper. Based on the geometrical information of defects and initial results obtained by PI-based analysis of defect reconstructions, a deep learning neural network model is built to reveal the physical relationship between defects and the noisy detection signals. This data-driven learning model is then applied to quantitatively assess and characterize defect profiles in structures, improve the accuracy of the analytical model and eliminate the impact of noise pollution in the process of inspection. To demonstrate advantages of the developed PIF for complex defect reconstructions with the capability of denoising, numerical examples including basic defect profiles, a stepped defect, a mixed-type defect have been examined. Results show that PIF has greater accuracy for reconstruction of defects in structures as compared with the analytical method and provides a valuable insight into the development of artificial intelligence-assisted inspection systems with high accuracy and efficiency in the fields of structural integrity and condition monitoring.

Key words: Physics-informed, Deep learning, Reconstruction of defect, Denoising

Chinese Library Classification O343

2010 Mathematics Subject Classification 74J05, 74J20, 74J25

1. Introduction

In non-destructive testing of elastic waveguide structures such as rods, plates, shells and beams, ultrasonic guided wave detection has the advantages of convenient excitation, long propagation distance, high sensitivity to defects and low energy consumption[1-4]. Especially for non-destructive testing in significant areas such as railway transportation, oil pipelines, aircraft airframe and wings[5], the high efficiency and high precision of ultrasonic guided wave detection are more important. Therefore, using guided waves for defect detection and reconstruction has been investigated by many researchers. As early as the beginning of this century, Rose[1] clarified that ultrasonic guided waves can be used to detect pores, weak cohesion and delamination, and have considerable reliability. Eremin *et al*.[6] studied the Lamb wave properties and its changes during the cyclic loading of CFRP sandwich panels with aluminium honeycomb core. Based on Lamb wave analysis, the fatigue failure and tensile-compressive failure of two specimens were identified. Puthillath *et al*.[7] developed a detection method of ultrasonic guided wave linear scanning, also known as G-scan, which can detect the bonding damage of the patch during the repair of the aircraft shell, such as adhesive and cohesive weaknesses similar to that found in adhesively bonded joints. Wang *et al*.[8] used the Born approximation to replace the total field near the defect with the incident field and then derived the mathematical relationship between the reflection coefficient located in the far field and the defect shape function in the form of Fourier transform pairs for the thinning defect reconstruction in the two-dimensional plate. Sikdar[9] used probabilistic damage detection algorithm to identify the location and size of the disband and high-density core region in a honeycomb composite sandwich structure(HCSS) utilizing ultrasonic guided waves and surface-bonded piezoelectric wafer transducers (PWTs). Da *et al*.[10] proposed a novel reference model-based method, called QDFT, for the quantitative reconstruction of pipeline defects using ultrasonic guided SH-waves in 2018. Based on the boundary integral equation, the Fourier transform pair of reflection coefficients in the wavenumber domain and the defect shape function in the spatial domain was analytically obtained using Born approximation to reconstruct the defect profiles.

Although many researchers have made valuable exploration and remarkable progress on the applications of guided waves for non-destructive testing to identify their values, it is difficult to realize high accurate and efficient defect reconstruction using the guided wave scattering theory due to the coupling of various modes in the guided wave scattering field. Moreover, the existing defect detection and reconstruction technologies need to cooperate with the signal processing system, the actual measurement is inevitably affected by environmental noise, which will lead to the inaccuracy of defect reconstruction. Therefore, it is time to revisit the artificial intelligent technology for reconstruction of defects with high levels of robustness and reliability.

Artificial intelligence(AI) has been rapidly developed and widely applied for solving many problems[11,12] with an impressive performance. In the field of defect detection, Munir *et al*[13] applied convolutional neural network for noisy ultrasonic signatures to improve classification performance of weldment defects and applicability. Xiaocen *et al*[14] proposed a rapid guided wave imaging method based on convolutional neural network (CNN) to quantitatively evaluate the corrosion damage. Also, artificial neural network was used for the efficient extraction and selection of features in the context of a decision support system[15]. Zhuang *et al*[16] proposed a novel deep morphological convolutional network (DMCNet) for feature learning of gearbox vibration signals for fault diagnosis. Virkkunen et al[17] developed a modern, deep convolutional network to detect flaws represented by phased-array ultrasonic data and they made extensive use of data augmentation to enhance the learning from initially limited raw data. Besides, Latête *et al*[18] used Faster R-CNN to identify, locate and size flat bottom holes (FBM) and side-drilled holes (SDH) in an immersed test specimen using a single plane wave insonification. Recently, a kernel-based machine learning model has been proposed to achieve automatic flaws detection, localization and characterization[19] and a dynamic radius support vector data description (DR-SVDD) has been proposed by Zhao *et al*.[20] for fault detection of aircraft engines. In the area of computer tomography(CT), Jin *et al*.[21] combined the deep convolutional neural network with the filtered back projection algorithm (FBP), which is the classical analytical models in image reconstruction. First, FBP was applied to process the sub-sampled sinogram for obtaining a preliminary reconstructed image, and then the reconstructed image as the input data was used to train the convolutional neural network for the output of a high-quality reconstructed image. In order to solve the problem of multiple scattering in image reconstruction, Sun *et al*.[22] divided the scattering inversion process into two steps: first, a theoretical model was employed to design a back propagation algorithm that was used to transform the data in the measurement domain into the image domain. Then, a deep convolutional neural network with U-net structure was generated as a scattering decoder to complete the reconstruction task using image domain data. The study found that the deep learning-based image reconstruction method has higher computational efficiency and reconstruction quality than other methods when dealing with multiple scattering problems. Boublil *et al*.[23] studied the combination of FBP algorithm and PWLS iterative algorithm with convolutional neural network to reconstruct images. It was concluded that the local fusion between these two algorithms can improve the balance between the resolution and the variance in the image reconstruction process, so it can improve the quality of the CT image. At the same time, two different types of image reconstruction methods (In the field of image reconstruction, FBP is a typical algorithm for directly negating forward operators, and PWLS is a typical iterative negation algorithm) in this study illustrated the universality of the local fusion of these algorithms. If the reconstruction algorithm changes, followed by modifying the subsequent neural network structure and then retraining it, the purpose of improving the quality of the reconstructed image can still be achieved. In[24], extensive research work using deep learning algorithms for scattering inversion was given, and it was concluded that in the field of image scattering inversion, due to the lack of sample data, the mainstream method of deep learning algorithms for scattering inversion was to combine the traditional reconstruction algorithm with the deep learning algorithm. Usually, traditional theoretical methods are used for pre-reconstruction, and then the reconstruction results as input data are collected to train the machine learning model for prediction of high-quality reconstruction results.

Considering the application of deep learning algorithms, especially the convolutional neural network algorithm in the field of image reconstruction, a quantitative defect reconstruction physics-informed framework (PIF) combining the existing theoretical model of guided wave defect reconstruction with deep learning algorithm is proposed in this paper. Using the results obtained by the PI-based analysis of defect reconstructions as training data, feature representations of defect profiles are extracted by an effective deep learning neural network, which is created using augmented datasets for its computational efficiency and robustness. To demonstrate the ability of the developed PIF for defect reconstructions in terms of the accuracy and denoising capability, numerical examples have been examined to evaluate the overall performance of the intelligent model by comparison of the published results.

2. PI-based analysis of defect reconstruction

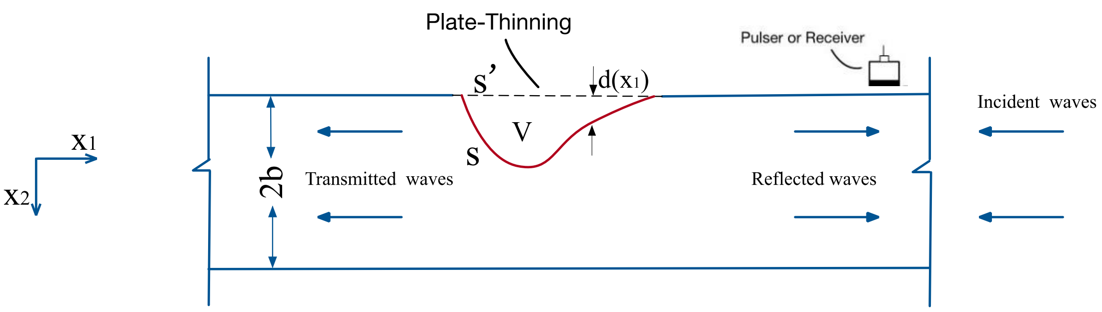

Fig.1 Reflection and transmission of an incident guided SH-wave by a plate thinning.

The process of incident waves travelling through the thinning structures can be described in Fig.1. First, the ultrasonic guided SH-wave is excited on the right side of the plate, and the reflection coefficient can be calculated from the reflected wave signal. Following this, the inverse Fourier transform of the reflection coefficient is then applied to analytically obtain the shape function of the defect for defect reconstruction[8]. The brief introduction of interactions occurred when waves propagate in cracked frame structures steps can be depicted as follows:

Assuming that the incident guided SH-wave in this problem has a single n*th* mode, propagating from right to left and being reflected back by the thinning part, and the reflected wave with the same mode as the incident wave mode is observed in the far field. Starting from the wave equation in the plate and the corresponding boundary conditions[8], the displacement field in the plate has been determined by Eq (1):

$$\tilde{u}^{\mathrm{inc}} = A_n^{\mathrm{inc}} f_n(\beta_n x_2) e^{+i\xi_n x_1} \quad , \quad \tilde{u}^{\mathrm{ref}} = A_n^{\mathrm{ref}} f_n(\beta_n x_2) e^{-i\xi_n x_1}$$

$$\beta_n = n\pi/2b,\ \xi_n = \sqrt{\frac{\omega^2}{V_s^2} - \beta_n^2} \tag{1}$$

where $\tilde{u}^{\mathrm{inc}}$ and $\tilde{u}^{\mathrm{ref}}$ depict the displacement fields of incident and reflected waves, respectively, n represents the nth guided SH-wave mode ($n = 0,1,2,\cdots$), A_n^{inc} and A_n^{ref} are the amplitude coefficients and $f_n(x)$ is defined as:

$$f_n(x) = \begin{cases} \cos x \ \text{ for } n = 0,2,4 \\ \sin x \ \text{for } n = 1,3,5 \end{cases} \tag{2}$$

Subsequently, the reflection coefficient is defined as the ratio of the two coefficients:

$$C^{\mathrm{ref}} = A_n^{\mathrm{ref}} / A_n^{\mathrm{inc}} \tag{3}$$

Applying the reciprocal theorem of dynamics[25] and the Green's function $\widetilde{U}(\boldsymbol{x}, \boldsymbol{X})$ in the plate, the scattered displacement field is analytically derived using the boundary integral equation:

$$\tilde{u}^{\mathrm{sca}}(\boldsymbol{x}) = \int_S [\tilde{u}^{\mathrm{tot}}(\boldsymbol{X}) \mu \frac{\partial \widetilde{U}(\boldsymbol{X}, \boldsymbol{x})}{\partial n(\boldsymbol{X})} - \mu \frac{\partial \tilde{u}^{\mathrm{tot}}(\boldsymbol{X})}{\partial n(\boldsymbol{X})} \widetilde{U}(\boldsymbol{X}, \boldsymbol{x})] ds(\boldsymbol{X}) \tag{4}$$

where $\tilde{u}^{\mathrm{sca}}$ and $\tilde{u}^{\mathrm{tot}}$ represent the scattered and total displacement fields, respectively. As the defect boundary is free, $\partial \tilde{u}^{tot}/\partial n = 0$ can be easily derived. For a weak scattering defect, the Born approximation can be applied to replace the total wave displacement field $\tilde{u}^{\mathrm{tot}}(\boldsymbol{X})$ in Eq.(4) with the incident wave field $\tilde{u}^{\mathrm{inc}}(\boldsymbol{X})$. One has

$$\tilde{u}^{\mathrm{sca}}(\boldsymbol{x}) \approx \int_S \tilde{u}^{\mathrm{inc}}(\boldsymbol{X}) \, \mu \frac{\partial \widetilde{U}(\boldsymbol{X}, \boldsymbol{x})}{\partial n(\boldsymbol{X})} ds(\boldsymbol{X}) \tag{5}$$

Using the Gauss theorem, the surface integral of the defect is converted into the integral over the volume of the defect：

$$\tilde{u}^{\mathrm{sca}}(\boldsymbol{x}) \approx \int_V \left[-k^2 \tilde{u}^{\mathrm{inc}}(\boldsymbol{X}) \mu \widetilde{U}(\boldsymbol{X}, \boldsymbol{x}) + \mu \frac{\partial \widetilde{U}(\boldsymbol{X},\boldsymbol{x})}{\partial X_i} \frac{\partial \tilde{u}^{\mathrm{inc}}(\boldsymbol{X})}{\partial X_i}\right] dV(\boldsymbol{X}) \tag{6}$$

where the Green's function $\widetilde{U}(\boldsymbol{x}, \boldsymbol{X})$ represents the anti-plane displacement at the field point $\boldsymbol{x} = (x_1, x_2)$ due to a harmonic point force exerted at the source point $\boldsymbol{X} = (X_1, X_2)$ in an intact plate. The Green's function $\widetilde{U}(\boldsymbol{x}, \boldsymbol{X})$ satisfies the equation of motion:

$$\nabla^2 \widetilde{U}(\boldsymbol{x}, \boldsymbol{X}) + k^2 \widetilde{U}(\boldsymbol{x}, \boldsymbol{X}) = -\delta(x - X)/\mu \tag{7}$$

And the traction free boundary condition can be written as:

$$\widetilde{T}(\boldsymbol{x}, \boldsymbol{X}) = \mu \frac{\partial}{\partial n(x)} \widetilde{U}(\boldsymbol{x}, \boldsymbol{X}) = 0 \text{ on } x_2 = \pm b \tag{8}$$

where $k = \omega / V_S$ is the shear wave number and $\partial/\partial n$ indicates the normal derivative. The solution to Eq.(7), that is the Green's function $\widetilde{U}(\boldsymbol{x}, \boldsymbol{X})$, can be expressed as:

$$\widetilde{U}(\boldsymbol{x}, \boldsymbol{X}) = \widetilde{U}^{\mathrm{inc}}(\boldsymbol{x}, \boldsymbol{X}) + \widetilde{U}^{\mathrm{ref}}(\boldsymbol{x}, \boldsymbol{X})$$

$$= \frac{1}{4\pi\mu} \int_{-\infty}^{\infty} \frac{e^{-R|x_2 - X_2|}}{R} e^{-i\xi(x_1 - X_1)} d\xi + \frac{1}{4\pi\mu} \int_{-\infty}^{\infty} (A^+ e^{-Rx_2} + A^- e^{+Rx_2}) e^{-i\xi(x_1 - X_1)} d\xi \tag{9}$$

where $\widetilde{U}^{\mathrm{inc}}(\boldsymbol{x}, \boldsymbol{X})$ is the fundamental solution; $\widetilde{U}^{\mathrm{ref}}(\boldsymbol{x}, \boldsymbol{X})$ means the additional term. $R = \sqrt{\xi^2 - k^2} (|\xi| \geq k) \; or \; i\sqrt{k^2 - \xi^2} \; (|\xi| \leq k)$.

Substituting Eq.(9) into Eq.(8), the undetermined amplitudes A^+ and A^- can be solved. Thus, $\widetilde{U}(\boldsymbol{x}, \boldsymbol{X})$ can be rewritten as:

$$\widetilde{U}(\boldsymbol{x}, \boldsymbol{X}) = \frac{1}{4\pi\mu} \int_{-\infty}^{\infty} \left[\frac{e^{-R|x_2 - X_2|}}{R} + \frac{e^{-2Rb}}{2R(1 + e^{-2Rb})} (e^{-RX_2} - e^{+RX_2})(e^{-Rx_2} - e^{+Rx_2}) + \right.$$

$$\left. \frac{e^{-2Rb}}{2R(1 - e^{-2Rb})} (e^{-RX_2} + e^{+RX_2})(e^{-Rx_2} + e^{+Rx_2})\right] e^{-i\xi(x_1 - X_1)} d\xi \tag{10}$$

For $|x_1| \gg |X_1|$, the far-field expression for the Green's function is given as

$$\widetilde{U}(\boldsymbol{x}, \boldsymbol{X}) \cong \widetilde{U}^{\mathrm{far}}(\boldsymbol{x}, \boldsymbol{X}) = \frac{i}{4b\mu\xi_0} e^{-i\xi_0|x_1 - X_1|} - \sum_j \frac{i}{2b\mu\xi_j} f_j(\beta_j x_2) f_j(\beta_j X_2) e^{-i\xi_j|x_1 - X_1|} \tag{11}$$

where the functions $f_n(x)$ is defined in Eq.(2).

Based on the far field approximation[8], the Green's function $\widetilde{U}(\boldsymbol{x}, \boldsymbol{X})$ in a traction-free plate waveguide for SH-wave can be expressed as:

$$\widetilde{U}(\boldsymbol{X}, \boldsymbol{x}) \approx \widetilde{U}^{\mathrm{far}}(\boldsymbol{X}, \boldsymbol{x}) = -\frac{i}{2b\mu\xi_n} \cos(\beta_n x_2) \cos(\beta_n X_2) e^{-i\xi_n(x_1 - X_1)} \tag{12}$$

Substituting Eq.(1) and (12) into Eq.(6), the displacement field of the reflected wave can be formulated as follows:

$$\tilde{u}^{\mathrm{ref}}(\boldsymbol{x}) = \frac{i}{2b} A_n^{\mathrm{inc}} \int_V \frac{\xi_n^2 + k^2 \cos(2\beta_n X_2)}{\xi_n} e^{2i\xi_n X_1} dV(\boldsymbol{X}) \times \cos(\beta_n x_2) e^{-i\xi_n x_1} \tag{13}$$

Comparing Eq.(1) with Eq.(13), it is noted that the integral term in Eq.(13) corresponds to the reflection coefficients, and the volume integral represents the multiple integrals. Thus, one obtain:

$$C^{\mathrm{ref}} = \frac{A_n^{\mathrm{ref}}}{A_n^{\mathrm{inc}}} = \frac{i}{2b}\frac{\xi_n^2+k^2}{\xi_n}\int_{-\infty}^{+\infty} d(X_1)e^{2i\xi_n X_1}dX_1 \tag{14}$$

where C^{ref} is the reflection coefficients and $d(X_1)$ describes the defect profile.

In Eq.(14), it can be observed that C^{ref} and $d(X_1)$ form a Fourier transform pair. Applying the inverse Fourier transform on Eq.(14), the defect profile $d(X_1)$ is determined by Eq.(15)

$$d(X_1) = \frac{1}{2\pi}\int_{-\infty}^{+\infty}\frac{-2ib\xi_n}{\xi_n^2+k^2}C^{\mathrm{ref}}e^{-2i\xi_n X_1}d(2\xi_n) \tag{15}$$

As $d(X_1)$ is described in the spatial domain and C^{ref} in the wavenumber domain, the defect reconstruction method aforementioned is called the wavenumber spatial transformation(WNST)[8]. To derive Eq.(15), there are some assumptions applied including the thinning defect as a weak scattering source $(d \ll b)$, Born approximation to replace the total field near the defect with the incident field, and the use of the far field approximation for calculating the Green function of the bounded plate. These approximations can help simplify the physics-informed formulations for defect reconstruction in an efficient way, while it is inevitable to introduce model errors and reduce the accuracy of reconstruction results.

3. A novel physics-informed framework

In order to improve the accuracy of the physics-informed modelling and eliminate the impact of noise pollution in the process of defect inspection and reconstruction, the fusion of a data-driven convolutional neural network (CNN) with the physics-informed analysis by the wavenumber spatial transformation method, called the WNSTConvNet framework, has been proposed in this paper for defect reconstruction.

The physical process of using ultrasonic waves to detect defects can be described as follows: In the process of propagation of sound waves along the medium, scattering will occur when encountering defects and this results in the transmission wave field and reflection wave field. Using the defect information from the transmitted and reflected signals, defect detection or reconstruction can be achieved. Therefore, guided wave defect reconstruction can be attributed to a scattering problem. For a scattering problem, it can be simply expressed by the following equation:

$$y = Tx + \xi \tag{16}$$

where x represents the scattering source that is assumed a thinning defect in this study, y represents the scattering field signal, T is an operator and its properties depend on the specific scattering problem, and ξ is the error. The task of inverse scattering problems is to calculate x based on y. The traditional methods to solve this class of problems are divided into two categories: The first group aims to directly construct the inverse problem model, such as the wavenumber spatial transformation method (WNST) aforementioned. The corresponding mathematical formulation can be given as follows:

$$x = \hat{T}^{-1} y \tag{17}$$

where $\hat{T}^{-1}$ is the theoretical reconstruction operator. The advantage of this method lies in that for the reconstruction of defects in simple structures, the calculation of the inverse scattering can be performed in a short time, while the disadvantage of this method could be difficult to obtain accurate results due to the ill-posed inverse problems. In particular, when the scattering problem becomes complex, it will be extremely difficult to develop the reconstructed model, therefore the reconstruction accuracy and reliability will be affected. The second class of methods for solving the inverse scattering problem is called the iterative-based method, such as the QDFT[10] and the mathematical formulation can be expressed as:

$$O\{y\} = \arg\min_{x} f(T\{x\}, y) \tag{18}$$

Where the function f is used to characterize the error between $T\{x\}$ and y. The iterative-based method has the ability to obtain accurate results and its disadvantage is that the efficiency of defect reconstruction is low due to a lot of computational time required by the iterative process.

In this paper, the approach based on machine learning is proposed to solve the inverse scattering problem. The inverse problem model, which is constructed through the training session, can be created in a mathematical form as follows:

$$L = \arg\min_{\theta} \sum_{n=1}^{N} M(x_n, H_\theta\{y_n\}) + r(\theta) \tag{19}$$

where x_n is the exact defect; y_n denotes the reflection coefficients; the symbol M is the loss function for characterizing the difference between samples x_n and $H_\theta\{y_n\}$; H_θ is the neural network built for solving the inverse problem, θ is the parameter in the neural network and is iteratively updated during the entire training process; N represents the total number of pairs in training samples; r is a regularization term, which prevents over-fitting and also limits the value of parameter θ to reduce the complexity of the trained network model H_θ. After training is completed, the network can achieve high reconstruction accuracy with a high level of efficiency.

In order to make full use of the existing defect reconstruction theory, the integration of the theoretical model (WNST) with machine learning methods is proposed in a manner of local fusion to efficiently and accurately solve defect reconstruction problem using the ultrasonic guided waves. The mechanism of this novel WNSTConvNet framework can be mathematically described as:

$$L = \arg\min_{\theta} \sum_{n=1}^{N} P(x_n, L_\theta\{\hat{T}^{-1} y_n\}) + g(\theta) \tag{20}$$

where the training sample pair is $(x_n, \hat{T}^{-1} y_n)$, in which x_n is the exact defect and $\hat{T}^{-1} y_n$ represents the defect constructed by the physics-informed construction model; The mean square error (MSE) is selected to evaluate the performance function P during the training session; L_θ is the WNSTConvNet framework, but its argument is the pre-reconstruction; L_2 regularization function is adopted to determine the regularization term $g(\theta)$ to reduce the complexity of the model and prevent overfitting. In this study, the initial results obtained by the physics-informed model are treated as training data for the generation of the machine learning model to improve the accuracy of defect reconstruction. The developed framework architecture and training process designed in this paper are shown in Fig.2.

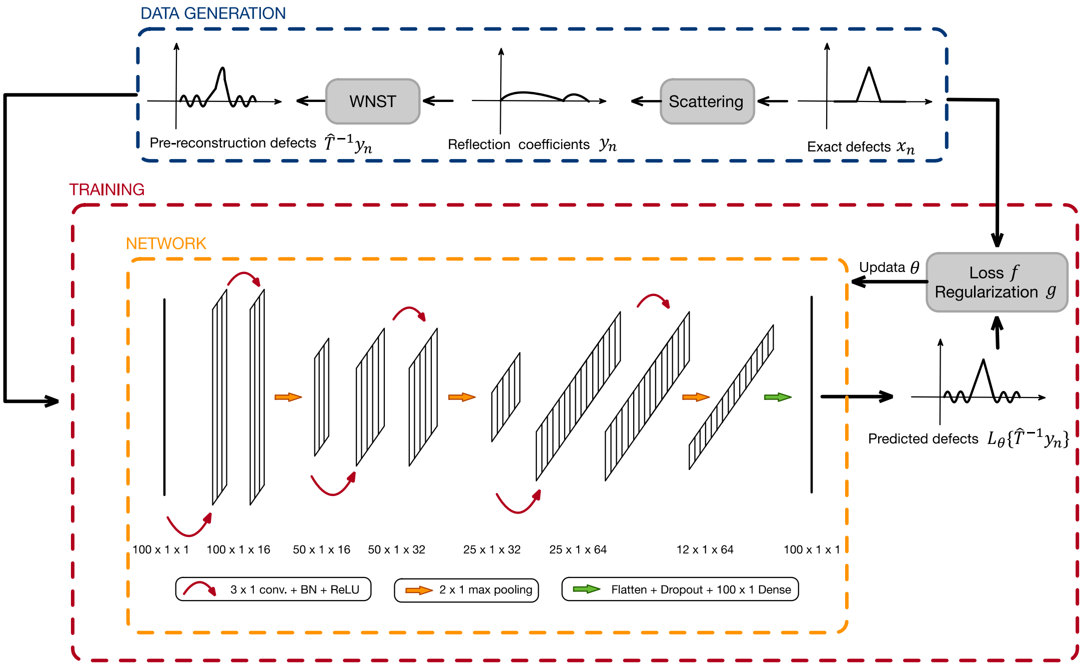

Fig.2 Schematic illustration of the reconstruction pipeline and the WNSTConvNet convolutional architecture. First, a set of reflection coefficients y_n have been calculated in the scattering process for the given different exact defects x_n. Then, the input of the reflection coefficients y_n for the theoretical model WNST has been to obtain the pre-reconstruction defects. Next, the pairs of $\{(x_n, \hat{T}^{-1} y_n)\}_{n=1}^{N}$ have been used to train the WNSTConvNet network L_θ with the performance function P and the regularization method g (L_2 regularization indeed).

Once the training is completed, the deep-learning network L_θ has the ability to efficiently predict the high-quality reconstruction of defects for an unknown defect signal $\hat{T}^{-1}y$.

Since the input samplings are one-dimensional signals, a one-dimensional deep learning network is constructed. The training process in Fig.2 could be described as follows: First, the pre-reconstructed defects $\hat{T}^{-1}y_n$ are obtained by WNST and utilized as the network inputs. Then, the mean square errors (MSE) between the exact defects x_n and the predicted profiles by the intelligent network are calculated to update the network parameter θ until the average MSE value of the entire sample set converges. Once the training session is completed, the deep-learning network has the ability to efficiently predict the high-quality reconstructed defect for a given defect signal $\hat{T}^{-1}y_n$. In this developed network, ReLU[26] activation function is used for each convolutional layer. In order to address the problem of gradient disappearance encountered during the training session, the batch normalization is performed before the activation[27] to improve the training efficiency. To prevent overfitting, a dropout layer[28] is added at the end of the network to discard some training parameters and improve its robustness. At the same time, L_2 regularization terms are applied to limit the training parameters and improve the generalization performance of the developed network for defect reconstruction. Based on the fusion of physics-informed calculations and predictions by deep-learning intelligent network, the developed WNSTConvNet framework which has been implemented in Python using the TensorFlow library[29] demonstrates the outperformance over its rivals for defect reconstructions throughout the complex examples in the following section.

4. Experimental validation

In this paper, two sets of sample data are generated to train the intelligent network in the WNSTConvNet framework for defect reconstruction with high levels of accuracy and robustness.

4.1. Data preparation

A mixed defect dataset that contains 1200 defect profiles including randomly isosceles triangular defects, rectangular defects and stepped defects, is created. Each type of predefined defect shapes comprises two groups of data: one is the input sample $\hat{T}^{-1}y_n$, and the other is the referenced real defect x_n. Each sample is represented as a vector with the dimension of 100×1, and the items in the vector depicts the depth information of the defect. For the input data of the WNSTConvNet framework, it is obtained by analytical calculations as follows: The reflection coefficients of the 0^{th} SH-wave mode corresponding to the exact defect are obtained by the modified boundary element method[30](MBEM) for all the examples in this paper. In practice, multi-dimensional Fourier Transforms and the frequency-wavenumber filtering can be applied for the incident wave removal and mode separation[31-32]. Following that, the shape function $d(X_1)$ of the defect is constructed by the wavenumber spatial transformation (Eqs.14-15), which deals with the input data required. Among 1200 sets of sampling data, the dataset split ratio (0.9) has been applied. That is to say, 900 samples are used for network training, 210 samples are used for the verification purpose during the training process and 90 samples are used for performing the unbiased evaluation of a final model once the training session is completed.

To further improve the performance of network and reconstruct more complex defect, the augmented dataset is generated. First, the pre-reconstruction isosceles triangular and rectangular defects with random sizes and shapes have been created using the wavenumber spatial transformation method formulated by Eqs. (14-15). Then, the augmented data has been generated by randomly shifting the signals in the horizontal direction. Summarily, there are 2800 sets of sampling data including 800 original inputs and 2000 augmented data for the network training, verification and testing.

4.2. Experimental results

Once the network training is completed, the reconstruction of defects with simple defective geometries, the stepped geometries and a mixed type of profiles will be conducted. In order to quantify the difference between the reconstructed defect and the real defect, the signal-to-noise ratio(SNR)[33] used as loss function to measure the reconstruction quality is proposed as follows:

$$SNR(\boldsymbol{x},\hat{\boldsymbol{x}}) \triangleq \max_{a\in R}\left\{10log_{10}\left(\frac{\|\boldsymbol{x}\|_{l2}^{2}}{\|\boldsymbol{x}-a\hat{\boldsymbol{x}}\|_{l2}^{2}}\right)\right\} \tag{21}$$

where $\boldsymbol{x}$ is the real defect, and $\hat{\boldsymbol{x}}$ is the predicted reconstruction of defect. A higher SNR value corresponds to a better reconstruction. Note that the vector $\boldsymbol{x}$ or $\hat{\boldsymbol{x}}$ used to characterize the defect shape in this study is actually the spatial distribution of the defect shape in the entire detection range, including the defect region and the defect-free region. The purpose of this proposed measure criteria lies in not only the investigation of the influence of the noise and error on the reconstructed defect quality in the defective area, but also the impact on the reconstruction result in the non-defective area.

4.2.1. A mixed dataset of defects

The convolutional neural network is initially constructed during the training session using the mixed type of defects described in Section 4.1. The reconstructed results of triangular defects, rectangular defects and stepped defects have been shown in Fig.3 and the SNR values obtained are provided in Table 1. It is noted that the WNSTConvNet framework has the ability to achieve defect reconstruction with a high level of accuracy. Especially, for rectangular and stepped defects, the SNR value reached about 28dB. The average SNR value of the reconstruction results across the entire testing dataset is 23.95dB, which enables the improvement of reconstruction results and leads to nearly 200% higher precision than the result by WNST.

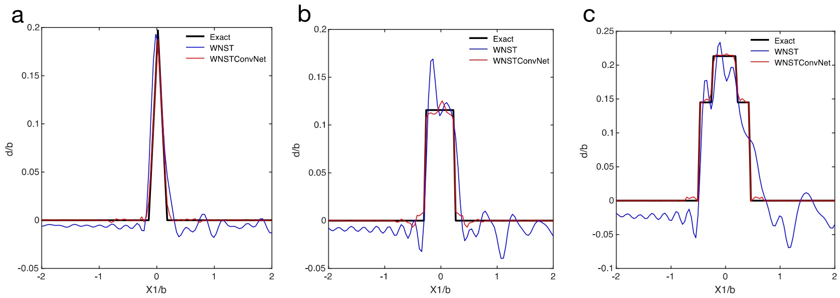

Fig.3 Reconstruct triangular defect (**a**), rectangular defect (**b**) and stepped defect (**c**) using the proposed WNSTConvNet framework

Table 1 Comparison of SNR (dB) values of reconstruction results of the two methods

Reconstruction methods	Triangular defects	Rectangular defects	Stepped Defects	Average SNR over the dataset
WNST	9.25	8.13	7.88	8.20
WNSTConvNet	20.29	28.40	28.03	23.95

4.2.2. Augmented datasets

Insufficient data is a critical issue that limits the application of machine learning methods in engineering subjects. In this situation, the generation of an augmented dataset by data augmentation method can fully dig out the information hidden owing to the limited data. In this experiment, the 2800 sets of augmented data have been used to train and verify the intelligent network. During the training session, the hyperparameters of the network have been finely tuned to reconstruct the asymmetric defects that are created by the combination of triangular and rectangular defects to improve the network with better generalization performance. The reconstruction results of two asymmetric combined defects have been shown in Fig.4a and Fig.4b. In Table 2, the obtained SNR values have been provided as compared to results from WNST. It can be observed that the network trained using triangular defects, rectangular defects, and their augmented data has the ability to reconstruct general asymmetric defects and the reconstruction accuracy has been remarkably improved by comparison of the results from the WNST method. It has been concluded that the network designed by the WNSTConvNet framework has demonstrated good generalization ability throughout the examples and the developed data-driven model that fuses the geometrical information of defects and initial results by the physics-informed analysis of defect reconstructions, has the capability to efficiently and effectively assess and characterize defects with complex profiles.

The major bottleneck in engineering applications of deep learning is the limited amounts of the effective data. In this study, the data-driven network model has been trained using defects with the basis profiles to realize the reconstruction of defects with complex profiles. However, it is very challenging to achieve the reconstruction with a high level of precision. In order to address this issue, additional 28 (about 1% of the original number of samples) defects with complex profiles representing the combination of triangular and rectangular shapes have been added to the training set for the improvement of the network with better generalization performance. This also empowers the network with the learning capability by taking the advantage of transfer learning[34].Therefore, there are 2828 sets of training data to build the effective machine learning model for the high-precision defect reconstruction. The reconstruction results of complex defect profiles have been shown in Fig.4c and the SNR value of the reconstruction result which is 22.52dB has been given in Table 3.

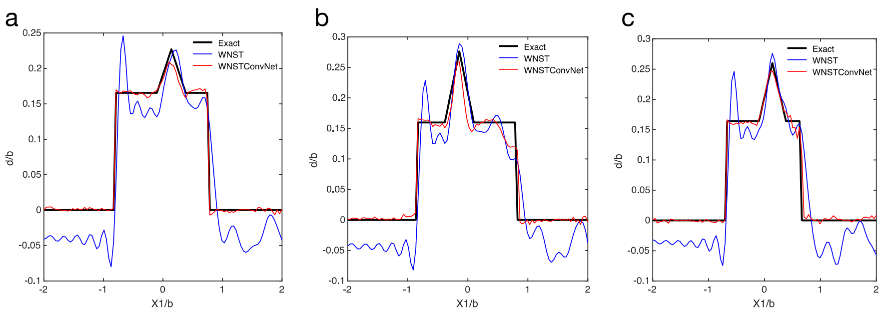

Fig.4 **a, b** Two reconstruction samples using neural network trained with 2800 augmentation samples. **c** Reconstruction result using neural network trained with 2828 augmentation samples which including 28 combination defects samples.

Table 2 Comparison of SNR (dB) values of reconstruction results of the two methods

Reconstruction methods	Sample a	Sample b	Average SNR over the dataset
WNST	8.79	8.87	7.54
WNSTConvNet	21.62	16.65	17.03

Table 3 SNR(dB) values of reconstruction results of neural network trained with additional 28 combination defects samples

Reconstruction methods	Sample c	Average SNR over the dataset
WNST	7.64	7.54
WNSTConvNet	22.52	21.33

4.2.3. Reconstruction of noisy defects

In order to ensure the robustness of this data-driven defect reconstruction model, the network trained by the augmented datasets, which include 2800 defect samples, is constructed to detect defects using signals in Gaussian white noise. First, Gaussian white noise with a signal-to-noise ratio of 15dB has been added to the input signals of WNSTConvNet, and then the trained deep-learning network has been examined for the denoising capability and defect reconstruction ability. In Fig.5a, defects with the noisy fringe and the predicted results by WNST and the developed deep-learning network have been provided. Table 4 shows the average SNR values (7.13dB and 13.86dB) of reconstructed results over the entire testing data by WNST and the WNSTConvNet framework, respectively. It is noted that the accuracy has been improved by nearly 100%, which demonstrates that the WNSTConvNet framework has great self-learning denoising capability. In order to further improve the denoising capability of the WNSTConvNet framework, a dataset of 2800 augmented signals containing 15dB of Gaussian white noise has been labelled as the training data to generate a more powerful, intelligent network. It can be observed that the denoising capability of the updated WNSTConvNet framework has been much improved as the reconstructed defect by the WNSTConvNet framework is in good agreement with the real defect and outperforms the result by WNST shown in Fig.5b and the accuracy of defect reconstruction can reach 17.66dB provided in Table 5.

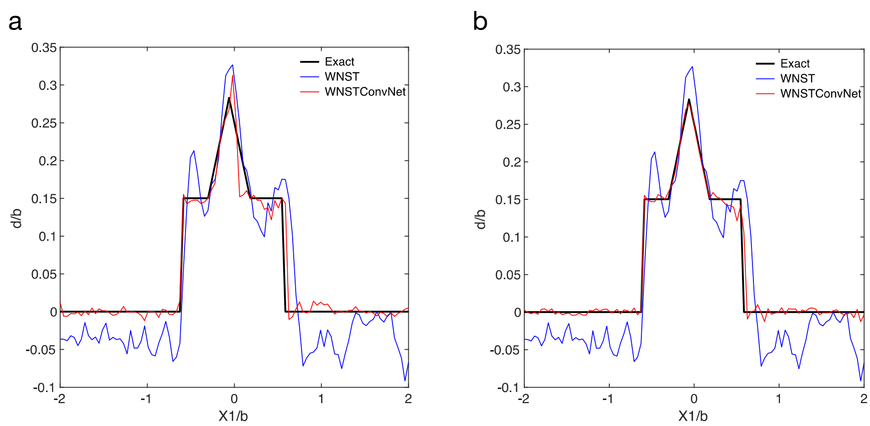

Fig.5 **a** Reconstruction result of defect from noisy signals using neural network trained with 2800 augmentation samples. **b** Reconstruction result of defect from noisy signals using neural network trained with 2800 augmentation noise-containing samples.

Table 4 SNR(dB) values of reconstruction results of defect from noisy signals using neural network trained with 2800 augmentation samples

Reconstruction methods	Sample a	Average SNR over the dataset
WNST	7.35	7.13
WNSTConvNet	14.62	13.86

Table 5 SNR(dB) values of reconstruction results of defect from noisy signals using neural network trained with 2800 augmentation noise-containing samples

Reconstruction methods	Sample b	Average SNR over the dataset
WNST	7.35	7.13
WNSTConvNet	18.04	17.66

5. Discussion

Simulation results prove the effectiveness and robustness of the WNSTConvNet framework for defect reconstruction with remarkable denoising capability. As compared with results by the WNST method based on the guided wave scattering theory, the WNSTConvNet framework which integrates the data-driven model with the physics-informed analysis has greater performance in terms of efficiency and denoising capability, while the reconstructed result is closer to the real defect profile. This is of great significance to the area of high-precision defect detection in engineering. At the same time, the great robustness of the WNSTConvNet framework can be demonstrated by the effective removal of samples mixed with noise during the defect reconstruction process. Therefore, it can improve the quality of reconstructed defects. On the other hand, removing the noise from the signals representing the features of the defect-free area also benefits the identification of the exact location of defects. It is noted that using the WNSTConvNet framework for reconstruction of defects, it takes less than one second to achieve the defect reconstruction with a high level of accuracy.

The limitation of the defect reconstruction method based on the supervised learning algorithm lies in the fact that the generated network architecture can only work on information that is either provided in the initial guess or extracted from the training data. For example, the neural network trained using the triangular datasets has a poor capability of prediction for reconstruction of rectangular defects. According to the first experimental test, one of the solutions to address this problem in practical applications is to train the neural network with datasets of a variety of typical geometrical information. Moreover, a classification layer followed by the reconstruction layer can be elaborately added in the design of network architecture so that the ensemble of different types of pre-reconstruction defects predicted by the corresponding convolutional neural network can be further developed in the network architecture for the improvement of computational accuracy. Another constraint on using neural networks to reconstruct defects is the need for a large amount of training data to guarantee the reliability of the predicted results. At present, the amount of relevant training data obtained from practical engineering applications is inadequate and the cost of obtaining data through experiments is also prohibitively expensive. Therefore, simulation results as a source of data to train a neural network is a feasible method in practice to solve data problems.

The WNSTConvNet framework proposed in this paper is the fusion of the physics-informed wave scattering analysis and the data-driven approach for defect reconstruction and its working mechanism has not been constrained by the type of theoretical model and the machine learning model. In this paper, the wavenumber spatial transformation(WNST) and the convolutional neural network (CNN) are selected as representative models to demonstrate the effectiveness and correctness of the proposed framework for reconstruction of complex defects.

6. Conclusion

This paper proposes a novel physics-informed quantitative defect reconstruction framework (WNSTConvNet), which integrates the wavenumber spatial transformation method (WNST) with a convolutional neural network in a local fusion manner. Throughout three complex experiments by comparison of the reconstruction results between WNSTConvNet and WNST, it has demonstrated that the WNSTConvNet framework is more effective, accurate and robust for reconstruction of complex defects. Results by WNSTConvNet have an average reconstruction accuracy of 20dB for the three types of defects, which demonstrates its good generalization performance. Especially, for the reconstruction of rectangular defects and stepped defects, the accuracy of reconstructions by WNSTConvNet has been improved by nearly 200% than the result by WNST. Moreover, considering the signal with Gaussian noise for the combined defect profiles, the WNSTConvNet framework has great denoising capability, which proves that the developed framework has good robustness for reconstruction of defects. Usually, the defect reconstruction process by WNSTConvNet can be completed within 1 second. Therefore, it’s a high-precision and high-efficiency quantitative defect reconstruction technique as compared to the analytical methods. In future work, experimental tests will be performed as an alternative to numerical simulations for the validation of the defect reconstruction method. Currently, the proposed framework has provided both useful guidelines to experimental tests throughout the numerical examples and valuable insights into the development of artificial intelligence-assisted inspection systems with high accuracy and efficiency in the fields of structural health monitoring and product life cycle prediction.

Acknowledgments

This work was supported in part by the State Key Laboratory of Mechanics and Control of Mechanical Structures at NUAA under Grant MCMS-E-0520K02, and in part by the Postgraduate Research & Practice Innovation Program of Jiangsu Province [grant number KYCX21_0184], and in part by the

Interdisciplinary Innovation Fund for Doctoral Students of Nanjing University of Aeronautics and Astronautics. The statements made herein are solely the responsibility of the authors.

Corresponding authors

Correspondence to dianzi.liu@uea.ac.uk and qianzh@nuaa.edu.cn

Availability of data and materials

The data that support the findings of this study are available on request from the corresponding author.

References

[1] ROSE, J. L. A baseline and vision of ultrasonic guided wave inspection potential. Journal of Pressure Vessel Technology, **124**, 273 (2002)

[2] BAI, H., SHAH, A. H., POPPLEWELL, N., & DATTA, S. K. Scattering of guided waves by circumferential cracks in composite cylinders. International Journal of Solids & Structures, **39**(17):4583-4603 (2002)

[3] SU, Z., YE, L., LU, Y. Guided Lamb waves for identification of damage in composite structures: A review. Journal of Sound and Vibration, **295**, 753-780 (2006)

[4] DA, Y.H., Wang, B., LIU, D.Z., QIAN, Z.H. An analytical approach to reconstruction of axisymmetric defects in pipelines using T(0, 1) guided waves[J]. Applied Mathematics and Mechanics(English Edition), (10) (2020)

[5] QIU, L., YUAN, S., MEI, H., FANG, F. An improved Gaussian mixture model for damage propagation monitoring of an aircraft wing spar under changing structural boundary conditions. Sensors, **16**, 291 (2016)

[6] EREMIN, A.V., BURKOV, M.V., BYAKOV, A.V., LYUBUTIN, P.S., PANIN, S.V., KHIZHNYAK, S.A. Investigation of acoustic parameters for structural health monitoring of sandwich panel under cyclic load. Key Engineering Materials, **712**, 319-323 (2016)

[7] PUTHILLATH, P., ROSE, J. L. Ultrasonic guided wave inspection of a titanium repair patch bonded to an aluminum aircraft skin. International Journal of Adhesion and Adhesives, **30**, 566-573 (2010)

[8] WANG, B., HIROSE, S. Inverse problem for shape reconstruction of plate-thinning by guided SH-waves. The Japanese Society for Non-Destructive Inspection, **53**(10): 1782-1789 (2012)

[9] SIKDAR, S., BANERJEE, S. Identification of disbond and high density core region in a honeycomb composite sandwich structure using ultrasonic guided waves. Composite Structures, **152**, 568-578 (2016)

[10] DA, Y., DONG, G., WANG, B., LIU, D., QIAN Z. A novel approach to surface defect detection. International Journal of Engineering Science,**133**(DEC.):181-195 (2018)

[11] ARRIDGE, S., MAASS, P. ÖKTEM, O., SCHONLIEB, C.B. Solving inverse problems using data-driven models. Acta Numerica, **28**, 1-174 (2019)

[12] AVCI, O., ABDELJABER, O., KIRANYAS, S., HUSSEIN, M., GABBOUJ, M., & INMAN, D. J. A review of vibration-based damage detection in civil structures: From traditional methods to machine learning and deep learning applications. Mechanical Systems and Signal Processing, **147**, 107077 (2021)

[13] MUNIR, N., KIM, H.J., PARK, J., SONG, S.J., KANG, S.S. Convolutional neural network for ultrasonic weldment flaw classification in noisy conditions. Ultrasonics, **94**, 74-81 (2019)

[14] WANG, X.C., LIN, M., LI, J., TONG, J.K., Huang, X.J., LIANG, L., FAN, Z., LIU, Y. Ultrasonic guided wave imaging with deep learning: Applications in corrosion mapping. Mechanical Systems and Signal Processing, **169**, 0888-3270 (2022)

[15] CRUZ, F.C., SIMASFILHO, E. F., ALBUQUERQUE, M. C. S., SILVA, I.C., FARIAS, C.T.T., GOUVEA, L.L. Efficient feature selection for neural network based detection of flaws in steel welded joints using ultrasound testing. Ultrasonics, **73**, 1-8 (2017)

[16] YE, Z., & YU, J. Deep morphological convolutional network for feature learning of vibration signals and its applications to gearbox fault diagnosis. Mechanical Systems and Signal Processing, **161**, 107984 (2021)

[17] VIRKKUNEN, I., KOSKINEN, T., JESSEN-JUHLER, O., RINTA-AHO, J. Augmented ultrasonic data for machine learning. Journal of Nondestructive Evaluation, **40**(1), 1-11 (2021)

[18] LATETE, T., GAUTHIER, B., BELANGER, P. Towards using convolutional neural network to locate, identify and size defects in phased array ultrasonic testing. Ultrasonics, **115**, 106436 (2021)

[19] MIORELLI, R., KULAKOVSKYI, A., CHAPUIS, B., D’ALMEIDA, O., MESNIL, O. Supervised learning strategy for classification and regression tasks applied to aeronautical structural health monitoring problems. Ultrasonics, **113**, 106372 (2021)

[20] ZHAO, Y.P., XIE, Y.L., YE, Z.F. A new dynamic radius SVDD for fault detection of aircraft engine. Engineering Applications of Artificial Intelligence, **100**, 104177 (2021)

[21] JIN, K.H., MCCANN, M.T., FROUSTEY, E., Unser, M. Deep convolutional neural network for inverse problems in imaging. IEEE Transactions on Image Processing, **26**(9), 4509-4522 (2017)

[22] SUN, Y., XIA, Z., KAMILOV, U.S. Efficient and accurate inversion of multiple scattering with deep learning. Optics express, **26**(11), 14678-14688 (2018)
[23] BOUBLIL, D., ELAD, M., SHTOK, J. ZIBULEVSKY, M. Spatially-adaptive reconstruction in computed tomography using neural networks. IEEE transactions on medical imaging, **34**(7), 1474-1485 (2015)
[24] MCCANN, M.T., JIN, K.H., UNSER, M. Convolutional neural networks for inverse problems in imaging: A review. IEEE Signal Processing Magazine, **34**(6), 85-95 (2017)
[25] ACHENBACH, J.A., ACHENBACH, J.D. Reciprocity in elastodynamics. Cambridge University Press (2003)
[26] NAIR, V., HINTON, G.E. Rectified linear units improve restricted boltzmann machines. In Icml, 807-814 (2010)
[27] IOFFE, S., SZEGEDY, C. Batch normalization: Accelerating deep network training by reducing internal covariate shift. In International conference on machine learning, (pp. 448-456). PMLR (2015)
[28] YOO, H.J. Deep convolution neural networks in computer vision: a review. IEIE Transactions on Smart Processing and Computing, **4**(1), 35-43 (2015)
[29] ABADI, M., AGARWAL, A., BARHAM, P., BREVDO, E., CHEN, Z., CITRO, C., ZHENG, X. Tensorflow: Large-scale machine learning on heterogeneous distributed systems. arXiv preprint arXiv:1603.04467 (2016)
[30] YANG, C., WANG, B., QIAN, Z. Three dimensional modified BEM analysis of forward scattering problems in elastic solids. Engineering Analysis with Boundary Elements, **122**, 145-154 (2021)
[31] FLYNN, E.B., CHONG, S.Y., JARMER, G.J., LEE, J.-R. Structural imaging through local wavenumber estimation of guided waves. NDT & E International **59**(7):1-1 (2013).
[32] CAI, J., SHI, L., QING, X.P. A time-distance domain transform method for Lamb wave dispersion compensation considering signal waveform correction. Smart materials and structures, **22**(10):105024 (2013)
[33] BOUBLIL, D., ELAD, M., SHTOK, J., ZIBULEVSKY, M. Spatially-adaptive reconstruction in computed tomography using neural networks. IEEE transactions on medical imaging, **34**(7), 1474-1485 (2015)
[34] OQUAB, M., BOTTOU, L., LAPTEV, I., SIVIC, J. Learning and transferring mid-level image representations using convolutional neural networks. In Proceedings of the IEEE conference on computer vision and pattern recognition, (pp. 1717-1724) (2014)